

Chemical stability and superconductivity in Ag-sheathed CaKFe₄As₄ superconducting tapes

Zhe Cheng,^{1,2} Chiheng Dong,^{1,*} He Huang,^{1,2} Shifa Liu,^{1,2} Yanchang Zhu,^{1,2} Dongliang Wang,¹ Vitalii Vlasko-Vlasov,³ Ulrich Welp,³ Wai-Kwong Kwok,³ Yanwei Ma^{1,2,*}

¹ Key Laboratory of Applied Superconductivity, Institute of Electrical Engineering, Chinese Academy of Sciences, Beijing 100190, China

² University of Chinese Academy of Science, Beijing, 100049, China

³ Argonne National Laboratory, 9700 South Cass Avenue, Argonne, Illinois 60439, USA

* E-mail address: dongch@mail.iee.ac.cn (C. Dong), ywma@mail.iee.ac.cn (Y. Ma)

Abstract

Ag-sheathed CaKFe₄As₄ superconducting tapes have been fabricated via the ex-situ powder-in-tube method. Thermal and X-ray diffraction analyses suggest that the CaKFe₄As₄ phase is unstable at high temperatures. It decomposes into the CaAgAs phase which reacts strongly with the silver sheath. We therefore sintered the tape at 500 °C and obtain a transport critical current density $J_c(4.2 \text{ K}, 0 \text{ T}) \sim 2.7 \times 10^4 \text{ A/cm}^2$. The pinning potential derived from magnetoresistance measurements is one order of magnitude lower than that of the (Ba/Sr)_{1-x}K_xFe₂As₂ tapes. Combining with the scanning electron microscopy and magneto-optical imaging results, we suggest that bad connectivity between superconducting grains caused by the low sintering temperature is the main factor responsible for the low J_c . However, this system is still a promising candidate for superconducting wires and tapes if we further optimize the post-annealing process to achieve better grain connectivity.

Introduction

The iron-based superconductors (IBSs) are of great interest from a basic point of view as well as in light of practical application [1]. In spite of the large varieties of IBSs with different crystal structures discovered so far, vortex pinning and anisotropy place fundamental restrictions on the current carrying ability. Furthermore, the high field performance of iron-based superconducting wires and tapes fabricated by the powder-in-tube (PIT) method [2] depends on other extrinsic factors, *i.e.* the purity of the precursors,

the compatibility to the sheath material, the density and texture of the superconducting core, and particularly, the homogeneity of the superconducting phase. After ten years of research and design, the optimally doped $(\text{Ba/Sr})_{1-x}\text{K}_x\text{Fe}_2\text{As}_2$ has emerged as the dominant material used in iron-based superconducting wires and tapes. On one hand, the quality of the $(\text{Ba/Sr})_{1-x}\text{K}_x\text{Fe}_2\text{As}_2$ precursor has progressively improved due to mature synthesis processes [3]. On the other hand, plenty of technologies, including flat rolling [4,5], cold [6,7] and hot [8] uniaxial pressing, hot isotropic pressing [9–11], as well as double sheath architecture [12] have been applied in the manufacturing process to enhance the texture and density of the superconducting core. Based on these efforts, the critical current density J_c of the $(\text{Ba/Sr})_{1-x}\text{K}_x\text{Fe}_2\text{As}_2$ superconducting tapes at 4.2 K and 10 T has been gradually improved and now surpasses the level needed for practical applications [13]. Nevertheless, like other doped IBSSs, the superconductivity of the BaK122 system is compromised by the non-uniformly distributed K atoms [14]. The inherent potassium clustering causes an inhomogeneous J_c distribution due to its sensitivity to K content [15]. It deteriorates the overall current carrying capability of the iron-based superconducting wires and tapes, especially at long lengths. Consequently, finding a non-doped, stoichiometric iron-based superconductor becomes vitally important for practical applications.

The recently discovered $\text{CaKFe}_4\text{As}_4$ superconductor is prominent among stoichiometric IBSSs owing to its high superconducting transition temperature of $T_c \sim 35$ K [16] which is competitive with the optimally K doped FeAs122 system. In contrast to the $(\text{Ca}_{0.5}\text{Na}_{0.5})\text{Fe}_2\text{As}_2$ solid solution with $I4/mmm$ space group, $\text{CaKFe}_4\text{As}_4$ possesses a $P4/mmm$ structure with the Ca and K layers alternately stacked between the Fe_2As_2 layers. Potassium doping on the alkaline earth element site unavoidably introduces substantial disorders whereas $\text{CaKFe}_4\text{As}_4$ is structurally ordered with Ca and K occupying different layers. In addition, there is no structural or magnetic phase transition [17], so one could consider this system as an optimally-doped ordered system. The upper critical field B_{c2} of the $\text{CaKFe}_4\text{As}_4$ single crystal is 71 T with the field parallel to the c axis and 92 T for the field perpendicular to the c axis [17]. The anisotropy parameter γ below 30 K is less than 2. The depairing current density J_0 at 0 K, estimated from $J_0 = \frac{\Phi_0}{3\sqrt{3}\mu_0\pi\xi\lambda^2}$, is 265 MA/cm², where Φ_0 is the flux quantum, $\xi=2.15$ nm is the coherence length, $\lambda=133$ nm is the penetration depth [18]. This J_0 -value is even larger than seen in other FeAs122

superconductors [19]. Further magnetic measurements on $\text{CaKFe}_4\text{As}_4$ single crystals indicate that the critical current density J_c at 10 T is nearly 1 MA/cm^2 with the field parallel to the c axis [20]. Moreover, it exhibits a more robust temperature dependence than the BaK122 counterpart, making it very promising to be used not only at liquid helium temperature, but also at intermediate temperatures accessible with cryocoolers.

In this paper, we synthesize the $\text{CaKFe}_4\text{As}_4$ precursor with a two-step method. The differential thermal analysis (DTA) on the precursor indicates a transition at $522 \text{ }^\circ\text{C}$ that is believed to be associated with the decomposition of the $\text{CaKFe}_4\text{As}_4$ phase. Therefore, we anneal the tape at $500 \text{ }^\circ\text{C}$ and achieve a J_c of $2.7 \times 10^4 \text{ A/cm}^2$ at 4.2 K and self-field. We demonstrate that bad connectivity between the superconducting grains due to low temperature sintering limits the overall critical current performance and indicate the need for a well-controlled post-annealing method to avoid the decomposition reaction in order to reach higher J_c in this system.

Experimental details

In order to improve the homogeneity, we synthesized the precursor according to a two-step method [3]. We firstly prepared the intermediate compounds with nominal compositions CaAs and KAs at $700 \text{ }^\circ\text{C}$ and $400 \text{ }^\circ\text{C}$, respectively. These intermediates were then mixed with Fe powders and As pieces according to the nominal composition $\text{Ca}_{1.15}\text{K}_{1.05}\text{Fe}_4\text{As}_4$. Excess CaAs and KAs were added to compensate for the loss of K and Ca during the heat treatment. The mixtures were ball milled for 10 hours in Ar atmosphere, sealed in a Nb tube afterwards and directly inserted into a preheated furnace at $900 \text{ }^\circ\text{C}$. After 30 hours of sintering, the Nb tube was quenched to room temperature [16]. Considering the strong reaction between Cu/Fe and iron-pnictides, we chose Ag as the outer sheath material. After grinding the $\text{CaKFe}_4\text{As}_4$ precursor into powders, we loaded them into a silver tube with outer and inner diameters of 8 mm and 5 mm, respectively. The tube was swaged, drawn and rolled into a 0.4 mm thick tape. We cut the tape into short samples and finally annealed them at temperatures between $500 \text{ }^\circ\text{C}$ and $800 \text{ }^\circ\text{C}$.

The X-ray diffraction (XRD) patterns of the precursor and the tapes were performed on a Bruker D8 Advance X-ray diffractometer. We analyzed the diffraction patterns by Rietveld refinement. The thermogravimetric (TG) and differential thermal analyses (DTA)

were performed on a Synchronous thermal analyzer (Netzsch; STA 499 F3) at a heating rate of 20 °C/min. The average composition of the superconducting core is determined by an electron probe micro-analyzer (EPMA). The transport critical current I_c was measured at 4.2 K via a four-probe method with a criterion of 1 $\mu\text{V}/\text{cm}$ at the High Magnetic Field Laboratory (CHMFL, Hefei). We measured the resistivity of the superconducting core on a Physical Property Measurement System (PPMS). The microstructure of the tape was analyzed by scanning electron microscopy (SEM, Zeiss SIGMA). The magneto-optical image (MOI) of the superconducting core was obtained using an optical cryostat (Montana Instruments) at Argonne National Laboratory. We polished the superconducting core after tearing off the silver sheath on that side. A Bi-substituted iron-garnet indicator film was placed in direct contact with the superconducting core as magnetic field sensor [21]. The magnetic field generated from a homemade cooper coil is applied with the direction perpendicular to the tape surface.

Results and discussion

Fig.1 shows the X-ray diffraction pattern of the $\text{CaKFe}_4\text{As}_4$ precursor. We find that most of the diffraction peaks can be well indexed with the $P4/mmm$ space group. There are additional reflections evidencing the presence of a small amount of residual Fe with $Im-3m$ structure. However, we find no trace of KFe_2As_2 that is usually seen in the ‘1144’ polycrystals. We thus perform Rietveld refinement with two phases. The refinement is successful as indicated by the reliability factors: $R_p=5\%$, $R_{wp}=6.59\%$. The fitted lattice parameters are $a=3.861\text{ nm}$ and $b=12.830\text{ nm}$. The calculated fractions of the $\text{CaKFe}_4\text{As}_4$ phase and the Fe phase are 97.2 % and 2.8 %, respectively. The EPMA measurements on 20 points of the superconducting core indicate that the average composition is $\text{Ca}_{0.97}\text{K}_{1.02}\text{Fe}_4\text{As}_4$, close to the nominal composition.

So far, scientists have found various stable 1144 systems with chemical formula $AeA\text{Fe}_4\text{As}_4$, where Ae and A are the alkaline-earth and alkaline elements, respectively. The large difference between the radii of the Ae and the A ions is necessary for the formation of the 1144 structure [16]. Song *et al.* further utilized density functional theory to study the stability of the 1144 system [22] and found that the $P4/mmm$ structure is sensitive to temperature and observe that $\text{CaKFe}_4\text{As}_4$ is only stable below a critical temperature of

$T' \sim 780$ K (507 °C). At higher temperatures, the 122 phase with $I4/mmm$ structure will dominate. In order to obtain a comprehensive understanding of the phase transition during the post-annealing process and evaluate a precise value of T' , we perform thermal gravity (TG) and differential thermal analysis (DTA) on the precursor. Fig.2 shows the TG and DTA curves of the precursor under an argon atmosphere. The loss of the mass due to the evaporation of potassium is not as evident until the temperature is close to the melting temperature $T_m \sim 950$ °C at which point there is a sharp endothermic peak. At intermediate temperature, there is a sharp exothermic peak at 522 °C, which is consistent with the theoretical prediction of the decomposition of the 1144 phase.

In order to verify this prediction, we annealed the $\text{CaKFe}_4\text{As}_4$ tapes in vacuum at different temperatures. As shown in Fig.3, all the diffraction peaks of the tape annealed at 500 °C for 0.5 hour can be well indexed with the $P4/mmm$ space group. There is no evidence for secondary phase. One can see a great enhancement of the intensities of the $(00l)$ peaks, suggesting strong c -axis texture. In order to quantitatively evaluate the c -axis texture, we utilize the Lotgering method to calculate $F = (\rho - \rho_0) / (1 - \rho_0)$ [23], where $\rho = \sum I(00l) / \sum I(hkl)$, $\rho_0 = \sum I_0(00l) / \sum I_0(hkl)$. I and I_0 are the intensities of every peak for the textured and randomly oriented samples, respectively. The calculated F value for the $\text{Ca}1144$ tapes annealed at 500 °C is 0.565, which is intermediate between the $\text{Sr}_{0.6}\text{K}_{0.4}\text{Fe}_2\text{As}_2$ superconducting tape [24] ($F \sim 0.476$) and the $\text{Ba}_{0.6}\text{K}_{0.4}\text{Fe}_2\text{As}_2$ superconducting tape [25] ($F \sim 0.590$). The large F value of the $\text{CaKFe}_4\text{As}_4$ tape indicates that the cold working process including drawing and rolling can effectively align the grains with the c -axis perpendicular to the tape surface. When the post-annealing temperature increases up to 700 °C, obvious minor phases appear in the diffraction pattern, namely the KFe_2As_2 and the CaAgAs phases, as shown in Fig. 3. Moreover, sintering at 800 °C largely suppresses the intensity of the $\text{CaKFe}_4\text{As}_4$ diffraction peaks, making KFe_2As_2 the predominant phase. Combining with the theoretical calculation and the DTA results, we suggest that there is a transition temperature between 500 °C and 700 °C, at which $\text{CaKFe}_4\text{As}_4$ decomposes into CaFe_2As_2 and KFe_2As_2 . Further continuous sintering above the transition temperature induces strong reaction between the Ag sheath and the CaFe_2As_2 at the interface. KFe_2As_2 is a superconductor with $T_c \sim 3.5$ K [26], while CaAgAs is a topological insulator [27]. These phases deteriorate the superconductivity of $\text{CaK}1144$ at

4.2 K and decrease the overall supercurrent. Therefore, different from the K-doped FeAs122 tapes which have a proper sintering temperature window ranging from 700 °C to 900 °C, we suggest that the CaKFe₄As₄ tapes can only be post-annealed below the critical temperature.

We measure the critical current of the CaKFe₄As₄ tapes annealed at different temperatures. As expected, all the tapes sintered at 700 °C and 800 °C shows no trace of supercurrents at 4.2 K. In contrast, we do observe a supercurrent in the tape post-annealed at 500 °C, as shown in Fig.4. At 0 T, the transport J_c is 2.7×10^4 A/cm² (critical current $I_c \sim 129$ A). With increasing field, the critical current density exhibits a strong field dependence and decreases to a value at 10 T that is nearly one-tenth of that at self-field. Furthermore, there is a clear hysteresis, indicating a weak-link effect in this sample. The transport J_c at 4.2 K and 10 T is 2.2×10^3 A/cm². This value is one order of magnitude larger than the 1111 [28] and Co-doped 122 rolled tapes [29], and much smaller than that of the K-doped 122 rolled tapes [3].

The main panel of Fig. 5(a) shows the temperature dependence of normalized resistance at 0 T. The silver sheath is peeled off before the measurement. With decreasing temperature, the resistance exhibits a metallic like behavior and suddenly drops at $T_c \sim 35$ K. The residual resistance ratio is $RRR = \rho(300\text{K})/\rho(35\text{K}) = 4.65$, close to that of the hot pressed Sr_{0.6}K_{0.4}Fe₂As₂ tapes [30]. However, the superconducting transition width $\Delta T_c \sim 5$ K is rather large, which may be caused by bad connectivity. As shown in the insets of Fig.5(a), the T_c^{onset} determined from the 90% criterion decreases very little with increasing field, while the T_c^{zero} defined with the 10% criterion is largely suppressed by the field, resulting in an obvious tail feature near T_c^{zero} . Fig.5(b) shows the B-T phase diagram. One can see the very steep temperature dependence of B_{c2} typically found in IBSs [31]. The slopes of the upper critical field, $-dB_{c2}/dT$, are 6.0 T/K and 9.7 T/K for the field perpendicular and parallel to the tape, respectively. These values are larger than that of the CaKFe₄As₄ single crystal, but close to the value of the powder sample [20]. The B_{c2} at 0 K determined with the Werthamer-Helfand-Hohenberg (WHH) formula is 242 T and 110 T for the field parallel and perpendicular to the tape surface, respectively. The anisotropy parameter of B_{c2} for fields applied perpendicular and parallel to the tape, $\gamma = B_{c2}^{\parallel} / B_{c2}^{\perp}$, is 2.32 near T_c and decreases to 1.86 at 33.4 K, as shown in the inset of Fig.5(b).

The tail structure in the magnetoresistance curves may imply a possible thermal activated flux flow (TAFF) behavior. According to the TAFF model, the resistivity can be expressed as $\rho(T, H)=2\rho_c U \exp(-U/T)/T$, where U is the thermally activated energy or pinning potential. Assuming that $\rho_{0f}=2\rho_c U/T$ is a temperature independent constant, the thermal activation energy is $U=U_0(1-T/T_c)$, and we can obtain the Arrhenius relation:

$$\ln\rho(T,H)=\ln\rho_{0f}-U_0(H)/T+U_0(H)/T_c=\ln\rho_0-U_0(H)/T,$$

where $\ln\rho_0=\ln\rho_{0f}+U_0(H)/T_c$. The pinning potential can be evaluated from the slope, $U_0(H)=-d\ln\rho/d(1/T)$. We depict the field dependences of U_0 for the two field directions in Fig.5(c). The pinning potential at 0.5 T with the field perpendicular to the tape is 650 K. It is much smaller than the K-doped 122 single crystal and tape [13,32], implying weak thermal barrier against vortex motion. The pinning potential shows a weak power-law field dependence, namely $U_0\propto B^{-n}$, with $n = 0.12$ and 0.14 for field perpendicular and parallel to the tape surface, respectively, manifesting a small anisotropy.

Fig.6(a) presents the optical image of the transverse section of the $\text{CaKFe}_4\text{As}_4$ tape showing a typical superconducting core with a saddle shape which arises due to the stronger deformation in the middle as compared to the two edges. Fig.6(b) shows a SEM image of the longitudinal section of the superconducting core. As a result of the low temperature sintering, the average size of the grains is as small as $2\ \mu\text{m}$. There are clearly observable voids and pores, limiting the actual current path along the tape. Fig.6(c) shows a MO image of the $\text{CaKFe}_4\text{As}_4$ superconducting tape. Magneto-optical images reveal the normal component of the magnetic induction, that is, the vortex density, at the imaged sample surface with a bright contrast representing high density. Note that in the current implementation this imaging technique does not distinguish between positive and negative vortices. The sample is cut into a rectangular shape with dimensions $4.08\times 3.20\times 0.18\ \text{mm}^3$. We firstly cool the sample to 5 K in zero field. Then we increase the field to 82.7 mT and decrease it to zero to prepare the sample in the remanent state. We can see two bright areas corresponding to the thickest sections of the superconducting core which trap a high vortex density. The transverse feathering feature may be due to residual damage and cracking arising in the rolling process. The bright contrast along the center-line of the sample represents negative vortices which are generated by the return field from the vortices trapped in the thicker sample sections on either side.

Conclusions

In summary, we have fabricated Ag-sheathed $\text{CaKFe}_4\text{As}_4$ tapes by ex-situ PIT method. We find that $\text{CaKFe}_4\text{As}_4$ is unstable at high temperature. It tends to decompose into CaFe_2As_2 , which strongly reacts with the silver sheath during the annealing process. Therefore, we sintered the tape at 500°C and obtained a self-field J_c of $2.7 \times 10^4 \text{ A/cm}^2$ at 4.2 K and self-field. The J_c exhibits a strong field dependence and decreases to $2.2 \times 10^3 \text{ A/cm}^2$ at 10 T. Magneto-transport and magneto-optical imaging reveal weak-link effects in the tape. The pinning potential derived from the magnetoresistance measurement is one order of magnitude smaller than that of the $\text{Ba}_{1-x}\text{K}_x\text{Fe}_2\text{As}_2$ tapes. Coupled with the SEM image, we conclude that bad connectivity between grains due to low temperature sintering is the main factor limiting the critical current at high fields. Considering the inherent high critical current density in the $\text{CaKFe}_4\text{As}_4$ single crystal, the polycrystalline wires and tapes are quite promising for practical application if a proper post-annealing process is applied to enhance the grain connectivity.

Acknowledgements

The authors would like to thank Dr. Fang Liu and Prof. Huajun Liu in High Magnetic Field Laboratory of the Chinese Academy of Sciences. We also thank Chen Li for help and useful suggestion. This work is partly supported by the National Natural Science Foundation of China (Grant No. 51320105015), the Beijing Municipal Science and Technology Commission (Grant No. Z171100002017006), the Bureau of Frontier Sciences and Education, Chinese Academy of Sciences (QYZDJ-SSW-JSC026), the Bureau of International Cooperation, Chinese Academy of Sciences (182111KYSB20160014) and Strategic Priority Research Program of Chinese Academy of Sciences (Grant No. XDB25000000). Magneto-optical work was carried out at Argonne National Laboratory and supported by the U.S. Department of Energy, Office of Science, Materials Sciences and Engineering Division.

Reference

- [1] Kamihara Y, Watanabe T, Hirano M and Hosono H 2008 Iron-Based Layered Superconductor $\text{La}[\text{O}_{1-x}\text{F}_x]\text{FeAs}$ ($x = 0.05\text{--}0.12$) with $T_c = 26$ K *J. Am. Chem. Soc.* **130** 3296–7
- [2] Hosono H, Yamamoto A, Hiramatsu H and Ma Y 2018 Recent advances in iron-based superconductors toward applications *Mater. Today* **21** 278–302
- [3] Dong C, Yao C, Lin H, Zhang X, Zhang Q, Wang D, Ma Y, Oguro H, Awaji S and Watanabe K 2015 High critical current density in textured Ba-122/Ag tapes fabricated by a scalable rolling process *Scr. Mater.* **99** 33–6
- [4] Zhang X, Oguro H, Yao C, Dong C, Xu Z, Wang D, Awaji S, Watanabe K and Ma Y 2017 Superconducting Properties of 100-m Class $\text{Sr}_{0.6}\text{K}_{0.4}\text{Fe}_2\text{As}_2$ Tape and Pancake Coils *IEEE Trans. Appl. Supercond.* **27** 7300705
- [5] Dong C., Yao C., Zhang X., Wang D. and Ma Y. 2018 Critical Current Density and Flux Pinning Mechanism in Flat-Rolled Sr-122/Ag Tapes *IEEE Trans. Appl. Supercond.* **28** 1–5
- [6] Togano K, Gao Z, Matsumoto A and Kumakura H 2013 Enhancement in transport critical current density of ex situ PIT Ag/(Ba, K) Fe_2As_2 tapes achieved by applying a combined process of flat rolling and uniaxial pressing *Supercond. Sci. Technol.* **26** 115007
- [7] Yao C, Lin H, Zhang X, Dongliang Wang, Zhang Q, Ma Y, Awaji S and Watanabe K 2013 Microstructure and transport critical current in $\text{Sr}_{0.6}\text{K}_{0.4}\text{Fe}_2\text{As}_2$ superconducting tapes prepared by cold pressing *Supercond. Sci. Technol.* **26** 075003
- [8] Lin H, Yao C, Zhang X, Dong C, Zhang H, Wang D, Zhang Q, Ma Y, Awaji S, Watanabe K, Tian H and Li J 2014 Hot pressing to enhance the transport J_c of $\text{Sr}_{0.6}\text{K}_{0.4}\text{Fe}_2\text{As}_2$ superconducting tapes *Sci. Rep.* **4** 6944
- [9] Weiss J D, Tarantini C, Jiang J, Kametani F, Polyanskii A A, Larbalestier D C and Hellstrom E E 2012 High intergrain critical current density in fine-grain $(\text{Ba}_{0.6}\text{K}_{0.4})\text{Fe}_2\text{As}_2$ wires and bulks *Nat. Mater.* **11** 682–5
- [10] Liu S, Lin K, Yao C, Zhang X, Dong C, Wang D, Awaji S, Kumakura H and Ma Y 2017 Transport current density at temperatures up to 25 K of Cu/Ag composite sheathed 122-type tapes and wires *Supercond. Sci. Technol.* **30** 115007
- [11] Pyon S, Suwa T, Park A, Kajitani H, Koizumi N, Tsuchiya Y, Awaji S, Watanabe K and Tamegai T 2016 Enhancement of critical current densities in $(\text{Ba},\text{K})\text{Fe}_2\text{As}_2$ wires and tapes using HIP technique *Supercond. Sci. Technol.* **29** 115002
- [12] Gao Z, Togano K, Matsumoto A and Kumakura H 2015 High transport J_c in magnetic fields up to 28 T of stainless steel/Ag double sheathed Ba122 tapes fabricated by scalable rolling process *Supercond. Sci. Technol.* **28** 012001
- [13] Zhang X, Yao C, Lin H, Cai Y, Chen Z, Li J, Dong C, Zhang Q, Wang D, Ma Y, Oguro H, Awaji S and Watanabe K 2014 Realization of practical level current densities in $\text{Sr}_{0.6}\text{K}_{0.4}\text{Fe}_2\text{As}_2$ tape conductors for high-field applications *Appl. Phys. Lett.* **104** 202601
- [14] Yeoh W K, Gault B, Cui X Y, Zhu C, Moody M P, Li L, Zheng R K, Li W X, Wang X L, Dou S X, Sun G L, Lin C T and Ringer S P 2011 Direct Observation of Local Potassium Variation and Its

Correlation to Electronic Inhomogeneity in $(\text{Ba}_{1-x}\text{K}_x)\text{Fe}_2\text{As}_2$ Pnictide *Phys. Rev. Lett.* **106** 247002

- [15] Dong C, Yao C, Huang H, Zhang X, Wang D and Ma Y 2017 Calorimetric evidence for enhancement of homogeneity in high performance $\text{Sr}_{1-x}\text{K}_x\text{Fe}_2\text{As}_2$ superconductors *Scr. Mater.* **138** 114–9
- [16] Iyo A, Kawashima K, Kinjo T, Nishio T, Ishida S, Fujihisa H, Gotoh Y, Kihou K, Eisaki H and Yoshida Y 2016 New-Structure-Type Fe-Based Superconductors: $\text{CaAFe}_4\text{As}_4$ ($A = \text{K}, \text{Rb}, \text{Cs}$) and $\text{SrAFe}_4\text{As}_4$ ($A = \text{Rb}, \text{Cs}$) *J. Am. Chem. Soc.* **138** 3410–5
- [17] Meier W R, Kong T, Kaluarachchi U S, Taufour V, Jo N H, Drachuck G, Ohmer A E B, Saunders S M, Sapkota A, Kreyssig A, Tanatar M A, Prozorov R, Goldman A I, Balakirev F F, Gurevich A, Ko S L B and Canfield P C 2016 Anisotropic thermodynamic and transport properties of single-crystalline $\text{CaKFe}_4\text{As}_4$ *Phys. Rev. B* **94** 064501
- [18] Cho K, Fente A, Teknowijoyo S, Tanatar M A, Joshi K R, Nusran N M, Kong T, Meier W R, Kaluarachchi U, On I G, Suderow H, Ko S L B, Canfield P C and Prozorov R 2017 Nodeless multiband superconductivity in stoichiometric single-crystalline $\text{CaKFe}_4\text{As}_4$ *Phys. Rev. B* **95** 100502
- [19] Mishev V, Nakajima M, Eisaki H and Eisterer M 2016 Effects of introducing isotropic artificial defects on the superconducting properties of differently doped Ba-122 based single crystals *Sci. Rep.* **6** 27783
- [20] Singh S J, Bristow M, Meier W R, Taylor P, Blundell S J, Canfield P C and Coldea A I 2018 Ultrahigh critical current densities, the vortex phase diagram, and the effect of granularity of the stoichiometric high- T_c superconductor $\text{CaKFe}_4\text{As}_4$ *Phys Rev Mater.* **2** 074802
- [21] Vlasko-Vlasov VK, Crabtree GW, Welp U, Nikitenko VI 1999 Magneto-optical studies of magnetization processes in high- T_c superconductors, PHYSICS AND MATERIALS SCIENCE OF VORTEX STATES, FLUX PINNING AND DYNAMICS, edited by Kossowsky R, Bose S, Pan V, Durusoy Z, Book Series: NATO ADVANCED SCIENCE INSTITUTES SERIES, SERIES E, APPLIED SCIENCES 356, 205-237
- [22] Song B Q, Nguyen M C, Wang C Z and Ho K M 2018 Stability of the 1144 phase in iron pnictides *Phys. Rev. B* **97**
- [23] Lotgering F K 1959 Topotactical reactions with ferrimagnetic oxides having hexagonal crystal structures—I *J. Inorg. Nucl. Chem.* **9** 113–23
- [24] Huang H, Yao C, Zhu Y, Zhang X, Dong C, Wang D, Liu S, Cheng Z, Awaji S and Ma Y 2018 Influences of Tape Thickness on the Properties of Ag-Sheathed $\text{Sr}_{1-x}\text{K}_x\text{Fe}_2\text{As}_2$ Superconducting Tapes *IEEE Trans. Appl. Supercond.* **28** 1–5
- [25] Cheng Z, Zhang X, Yao C, Dong C, Wang D, Huang H, Liu S and Ma Y 2018 Effect of wire diameter on the microstructure and J_c properties of $\text{Ba}_{0.6}\text{K}_{0.4}\text{Fe}_2\text{As}_2$ tapes *IEEE Trans. Appl. Supercond.* **28** 1–5
- [26] Liu Y, Tanatar M A, Kogan V G, Kim H, Lograsso T A and Prozorov R 2013 Upper critical field of high-quality single crystals of KFe_2As_2 *Phys. Rev. B* **87** 477
- [27] Nayak J, Kumar N, Wu S-C, Shekhar C, Fink J, Rienks E D L, Fecher G H, Sun Y and Felser C 2018 Electronic properties of topological insulator candidate CaAgAs *J. Phys. Condens. Matter* **30**

045501

- [28] Zhang Q, Zhang X, Yao C, Huang H, Wang D, Dong C, Ma Y, Ogino H and Awaji S 2017 Enhanced transport critical current density in Sn-added $\text{SmFeAsO}_{1-x}\text{F}_x$ tapes prepared by the PIT method *Supercond. Sci. Technol.* **30** 065004
- [29] Dong C, Yao C, Huang H, Wang D, Zhang X and Ma Y 2017 Superconducting Properties of PIT $\text{BaFe}_{2-x}\text{Co}_x\text{As}_2$ Tapes *IEEE Trans. Appl. Supercond.* **27** 1–4
- [30] Dong C, Lin H, Huang H, Yao C, Zhang X, Wang D, Zhang Q, Ma Y, Awaji S and Watanabe K 2016 Vortex pinning and dynamics in high performance $\text{Sr}_{0.6}\text{K}_{0.4}\text{Fe}_2\text{As}_2$ superconductor *J. Appl. Phys.* **119** 143906
- [31] Gurevich A 2011 To use or not to use cool superconductors? *Nat. Mater.* **10** 255–9
- [32] Wang X-L, Ghorbani S R, Lee S-I, Dou S X, Lin C T, Johansen T H, Müller K-H, Cheng Z X, Peleckis G, Shabazi M, Qviller A J, Yurchenko V V, Sun G L and Sun D L 2010 Very strong intrinsic flux pinning and vortex avalanches in $(\text{Ba},\text{K})\text{Fe}_2\text{As}_2$ superconducting single crystals *Phys. Rev. B* **82** 024525

Fig.1. Powder XRD pattern and Rietveld refinement of the $\text{CaKFe}_4\text{As}_4$ precursor.

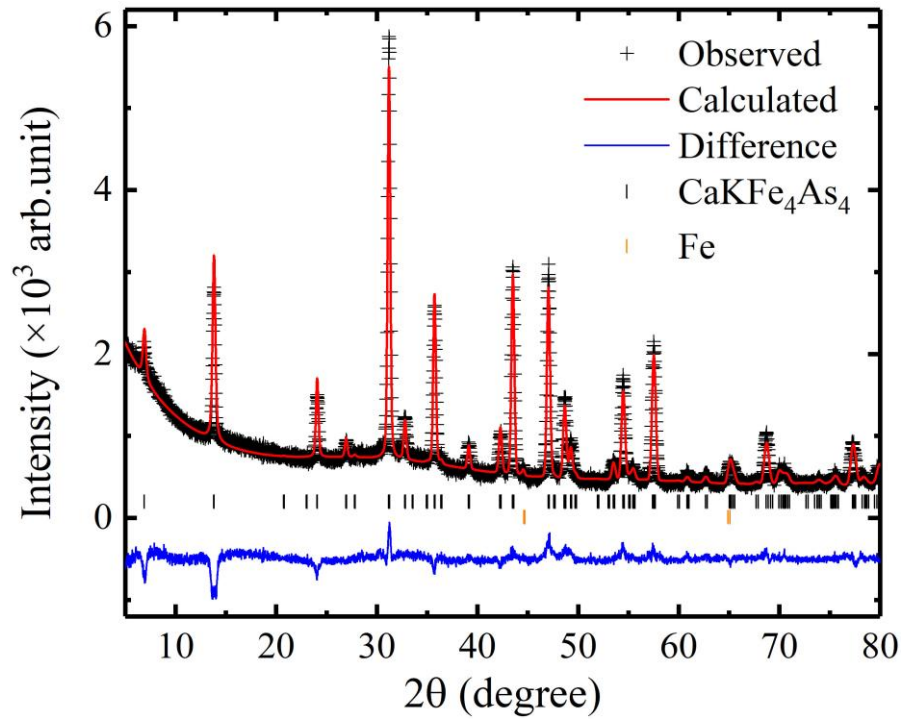


Fig.2. TG and DTA curves of the $\text{CaKFe}_4\text{As}_4$ precursor.

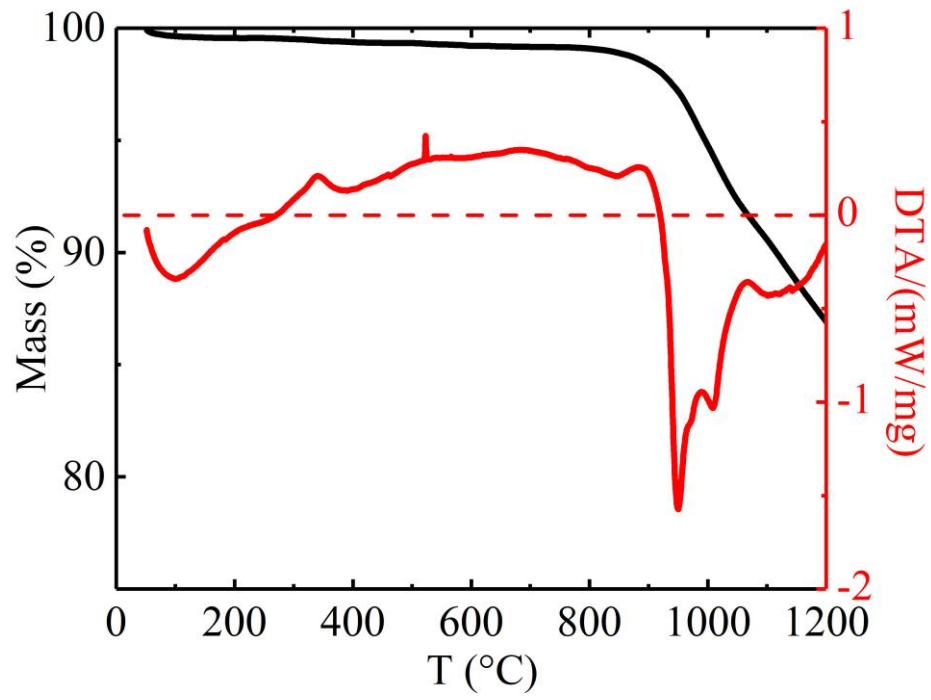


Fig.3. XRD patterns of the $\text{CaKFe}_4\text{As}_4$ superconducting tapes sintered at $500\text{ }^\circ\text{C}$, $700\text{ }^\circ\text{C}$ and $800\text{ }^\circ\text{C}$.

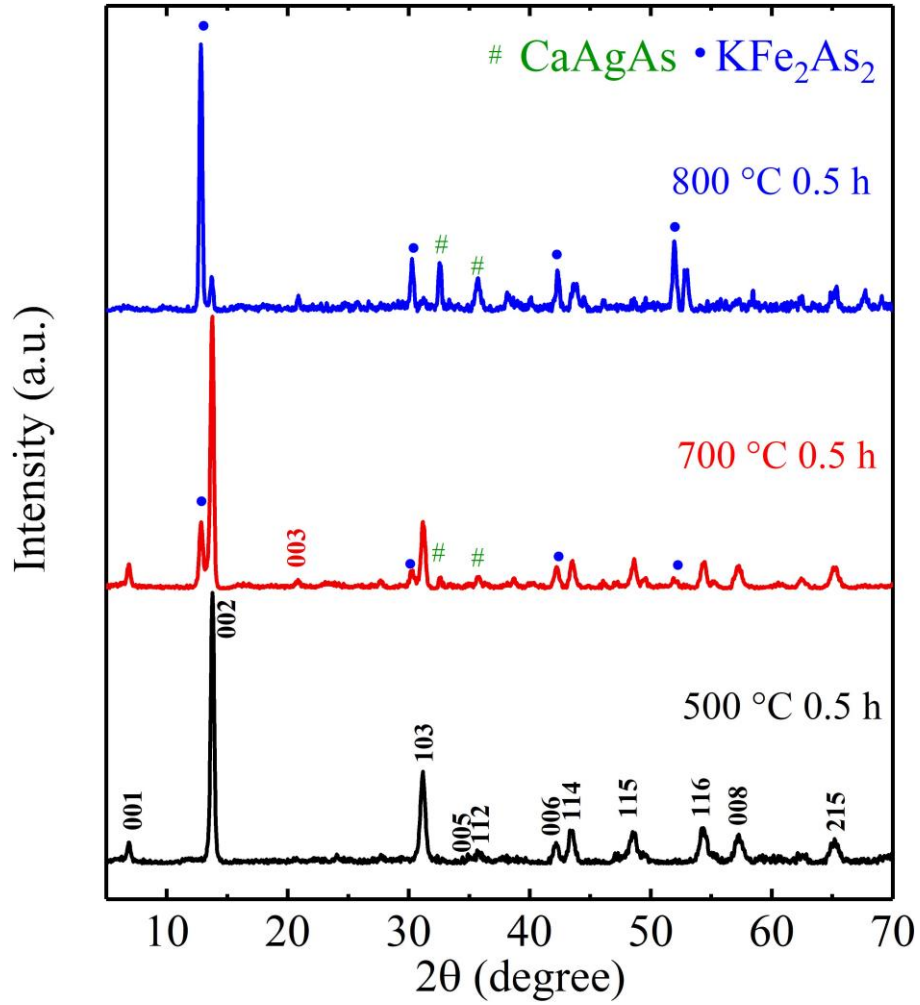


Fig.4. Magnetic field dependence of the transport J_c at 4.2 K with increasing and decreasing field for the $\text{CaKFe}_4\text{As}_4$ tapes sintered at 500 °C for 0.5 h.

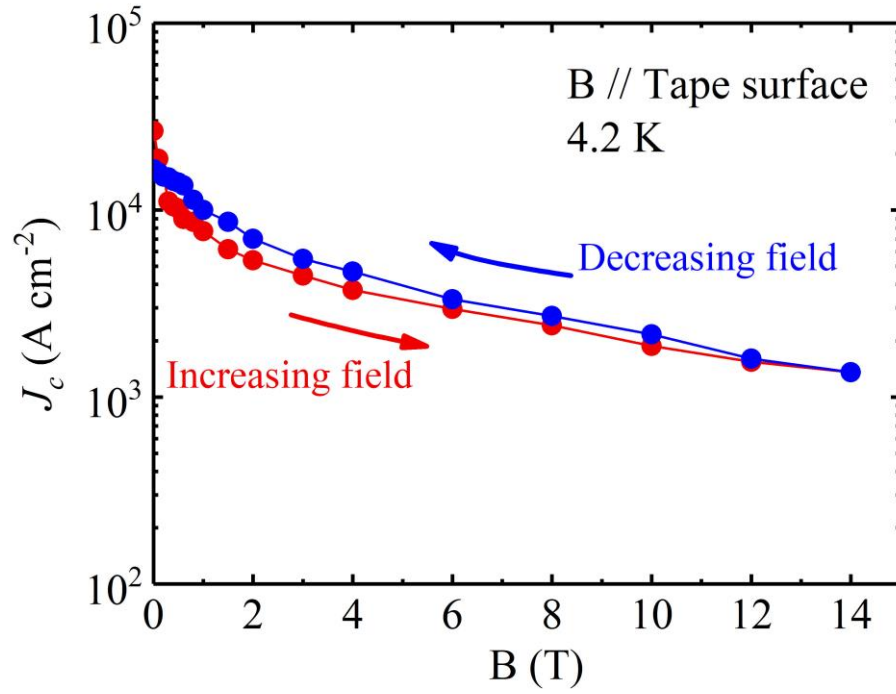


Fig.5. (a) Temperature dependence of the normalized resistance for the $\text{CaKFe}_4\text{As}_4$ tapes. Inset shows the magnetoresistance near T_c with $H \perp$ tape and $H \parallel$ tape. (b) B-T phase diagram, the inset is the anisotropy parameter as a function of temperature. (c) Field dependences of pinning potential for $H \perp$ tape and $H \parallel$ tape.

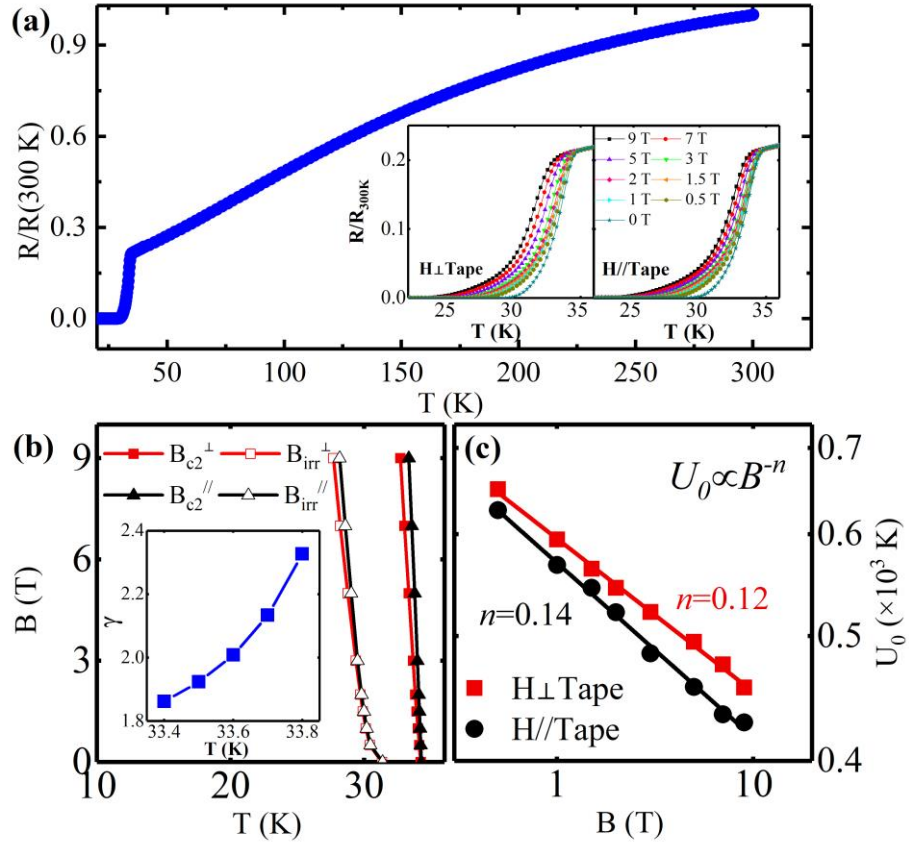


Fig.6. (a) Optical image of the transverse cross-section of the $\text{CaKFe}_4\text{As}_4$ tapes. (b) SEM image of the longitudinal section of the superconducting core. (c) MO image of the superconducting core. In this image the tape axis is vertical.

